Microdomains bounded by endoplasmic reticulum segregate cell cycle calcium transients in syncytial *Drosophila* embryos

Huw Parry, Alex McDougall, and Michael Whitaker

Institute for Cell and Molecular Biosciences, University of Newcastle upon Tyne Medical School, Newcastle upon Tyne NE2 4HH, England, UK

Cell cycle calcium signals are generated by the inositol trisphosphate ($InsP_3$)–mediated release of calcium from internal stores (Ciapa, B., D. Pesando, M. Wilding, and M. Whitaker. 1994. *Nature*. 368:875–878; Groigno, L., and M. Whitaker. 1998. *Cell*. 92:193–204). The major internal calcium store is the endoplasmic reticulum (ER); thus, the spatial organization of the ER during mitosis may be important in shaping and defining calcium signals. In early *Drosophila melanogaster* embryos, ER surrounds the nucleus and mitotic spindle during mitosis, offering an opportunity to determine whether perinuclear localization of ER conditions calcium signaling during mitosis. We establish that the nuclear divisions in syncytial *Drosophila* embryos are accompanied by both cortical and nuclear localized calcium transients. Constructs that chelate $InsP_3$ also prevent nuclear division. An analysis of nuclear calcium concentrations demonstrates that they are differentially regulated. These observations demonstrate that mitotic calcium signals in *Drosophila* embryos are confined to mitotic microdomains and offer an explanation for the apparent absence of detectable global calcium signals during mitosis in some cell types.

Introduction

Calcium signals have been shown to play an important regulatory role in controlling the cell division cycle of early sea urchin (Ciapa et al., 1994; Wilding et al., 1996; Groigno and Whitaker, 1998), frog (Miller et al., 1993; Snow and Nuccitelli, 1993; Muto et al., 1996), and mammalian embryos (Tombes et al., 1992; Nixon et al., 2002). Cell cycle calcium signals activate calmodulin (Lu and Means, 1993; Takuwa et al., 1995; Török et al., 1998), and calmodulin kinase II is required for mitosis in both sea urchin embryos (Baitinger et al., 1990) and somatic cells (Patel et al., 1999). Nonetheless, despite clear evidence that blocking calcium signals prevents mitosis, in many cases, putative mitotic calcium signals are small or undetectable (Tombes and Borisy, 1989; Kao et al., 1990; Tombes et al., 1992; Wilding et al., 1996; Whitaker and Larman, 2001). The absence of calcium signals during mitosis in some higher eukaryotic cell types under some conditions implies that calcium regulation of mitosis is not a universal signaling mechanism in higher eukaryotes.

Correspondence to Michael Whitaker: michael.whitaker@ncl.ac.uk

Abbreviations used in this paper: CaGr, calcium green dextran; $[Ca_i]$, intracellular free calcium concentration; $DiIC_{18}$, 1,1′-dioctadecyl-3,3,3′,3′-tetramethylindocarbocyanine perchlorate; $InsP_3$, inositol trisphosphate; NEB, nuclear envelope breakdown; TMR, tetramethylrhodamine.

The source of calcium for signals during mitosis is the ER (Ross et al., 1989; Ciapa et al., 1994). The ER gathers around the nucleus as mitosis approaches and is closely associated with the mitotic spindle (Harel et al., 1989). The ER–spindle complex can be isolated and shown to sequester calcium (Silver et al., 1980). ER membranes pervade the mitotic spindle (Harris, 1975), so is possible that calcium released very locally to calcium-binding sites over micron length scales may provide signals at the chromosomes and spindle poles. Very local signals of this kind are probably not detectable with current imaging technologies.

During the early syncytial nuclear divisions of *Drosophila melanogaster* embryos, ER becomes highly concentrated around the nucleus at prophase and is very closely associated with the spindle poles; however, the ER does not invade the spindle itself (Bobinnec et al., 2003). This circumstance offers the opportunity to image calcium concentrations within the nucleus and mitotic spindle without the complication of colocalized ER. It also offers the opportunity to test whether the interaction between ER and mitotic spindle creates a calcium-signaling environment that is distinct from bulk cytoplasm.

The amenable genetics of *Drosophila* has allowed the identification of a plethora of gene products that are directly

The Journal of Cell Biology, Vol. 171, No. 1, October 10, 2005 47–59
http://www.jcb.org/cgi/doi/10.1083/jcb.200503139

involved in regulating the cell division cycle (Gonzalez et al., 1994; Sullivan and Theurkauf, 1995). Many are homologues of regulators that are important in controlling mammalian cell cycles. A number of cell cycle regulatory genes were first identified through their effects on the cell cycles of various early embryos (Evans et al., 1983; Gautier et al., 1988; Sunkel and Glover, 1988; Glover et al., 1991, 1995; Edgar and Lehner, 1996). Calcium gradients may help determine the dorso–ventral axis in *Drosophila* (Creton et al., 2000), but nothing is known about calcium signaling in the fly's early embryonic cell cycles. In this study, we demonstrate that calcium regulates nuclear division during early embryonic cell cycles and go on to show that the ER surrounding the nuclear compartment encloses a calcium-signaling microenvironment that controls mitosis.

Results

Early *Drosophila* development is marked by 13 rapid nuclear divisions that occur in the same cytoplasm without cytokinesis (Foe and Alberts, 1983; Foe et al., 1993). Dividing nuclei are first located deep within the embryo; they migrate to the embryo cortex during cycles 8 and 9, and nuclei divide just beneath the surface of the embryo during cycles 10–13. During cycles 10–13, superficial nuclei undergo mitosis asynchronously, giving appearance to mitotic waves that originate simultaneously at both anterior and posterior embryonic poles. At 25°C, the waves move from pole to equator in ~30 s, as determined in fast-frozen embryos (Foe and Alberts, 1983). At 18°C, we find that the mitotic waves are substantially slower, whereas

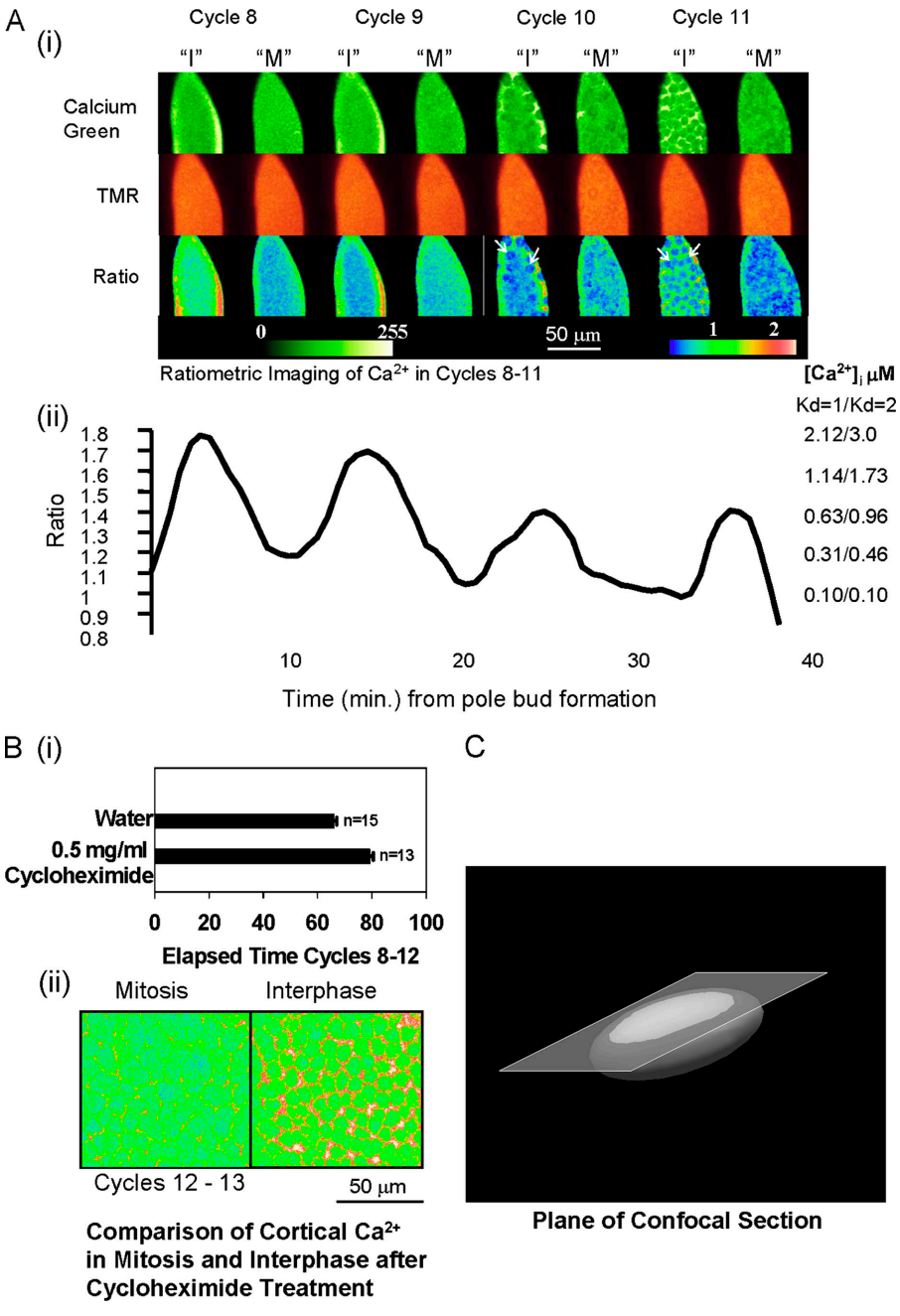

Figure 1. **Calcium increases in phase with the interphase cortical contractions in syncytial *Drosophila* embryos.** (A i) $[Ca_i]$ increases measured by confocal ratio imaging. The three rows of images display CaGr, TMR, and ratio images that represent the spatial distribution of the calcium signals as snapshots in mid-interphase and midmitosis. Interphase and mitosis in cycles 8 and 9 are inferred from the timing of the cortical contractions (I and M). In the later two cycles, when the nuclei have come to the egg cortex, their presence is marked by areas of low calcium concentration. They are sometimes faintly visible in the ratiometric image (arrows), and the correlation between nuclei in interphase (I), the cortical contractions, and the calcium increase was noted. The pixel values in the ratiometric image are represented by a conventional rainbow scale, with higher calcium concentrations shown as warmer tones. Red colors in the image correspond to $[Ca_i]$ in the midmicromolar range, as can be seen by comparison with the calibration shown in (ii). (ii) The temporal pattern of $[Ca]_i$ increase in the embryo shown in (i). $[Ca_i]$ values are means for the whole embryo. Calibrated calcium concentrations are shown at right (see Calibration...signals). Note that as the nuclear division cycle time lengthens, the time between $[Ca_i]$ signal peaks also lengthens so that the $[Ca_i]$ signal remains in phase with the nuclear cycle. (B i) The nuclear division cycle length can be increased experimentally by ~20% through treatment with cycloheximide. Numbers on x axis represent minutes. Error bars represent SEM. (ii) The $[Ca]_i$ peaks remain associated with interphase after cycloheximide treatment. Temperature is 18°C. (C) A schematic view of the embryo showing the plane of the confocal section in this and other figures. Note that the periphery of the section through the embryo provides images of the cortex and that the center of the section looks deeper into the embryo. Images are oriented with the anterior pole being uppermost.

Table I. **Mean peak and trough [Ca_i] in cortical confocal sections in cycles 8–13**

	Cycle 8	Cycle 9	Cycle 10	Cycle 11	Cycle 12	Cycle 13
Trough						
Ratio	1.03 ± 0.019	1.02 ± 0.014	1.02 ± 0.025	1.00 ± 0.013	1.00 ± 0.015	1.00 ± 0.009
[Ca_i] (μM)	0.13 ± 0.018	0.12 ± 0.013	0.12 ± 0.023	0.10 ± 0.012	0.10 ± 0.013	0.10 ± 0.008
Peak						
Ratio	1.56 ± 0.100	1.57 ± 0.112	1.34 ± 0.025	1.38 ± 0.042	1.36 ± 0.058	1.23 ± 0.033
[Ca_i] (μM)	1.01 ± 0.305	1.04 ± 0.354	0.52 ± 0.042	0.59 ± 0.078	0.55 ± 0.103	0.35 ± 0.044
n	4	6	10	10	8	3

Assumes K_d of 1 μM for CaGr.

cycle times are only slightly lengthened, allowing the waves to be imaged much more readily with confocal microscopy.

Calcium changes occur in syncytial *Drosophila* embryos in fixed phase relation with the nuclear division cycle

Fig. 1 A shows fluorescence signals in a *Drosophila* embryo as it passes through cell cycles 8–11. Increased intracellular free calcium concentration ([Ca_i]) is detected by quantitative ratiometric imaging in each cell cycle as nuclei enter interphase. The ratio of calcium green dextran (CaGr) and rhodamine dextran fluorescence quantitatively reflects the intracellular calcium concentrations at different points within the confocal section. Red colors represent ≥1 μM calcium, yellow colors represent 0.5–1 μM, green colors represent 0.1–0.5 μM, and blue colors represent concentrations <0.1 μM (calibration shown in Fig. 1 A ii). [Ca_i] falls during mitosis and is elevated in the cortex of the embryo. Nuclei migrate to the cortex of the embryo during cycle 10. Once the nuclei enter the confocal section, [Ca_i] is seen in the ratiometric images to be highest around the nuclei in interphase, but it does not increase to the same degree within the nuclei, which appear as circular voids. In these and other images, the plane of confocal section passes through the embryo cortex at the edges of the image, whereas the center of the image represents areas

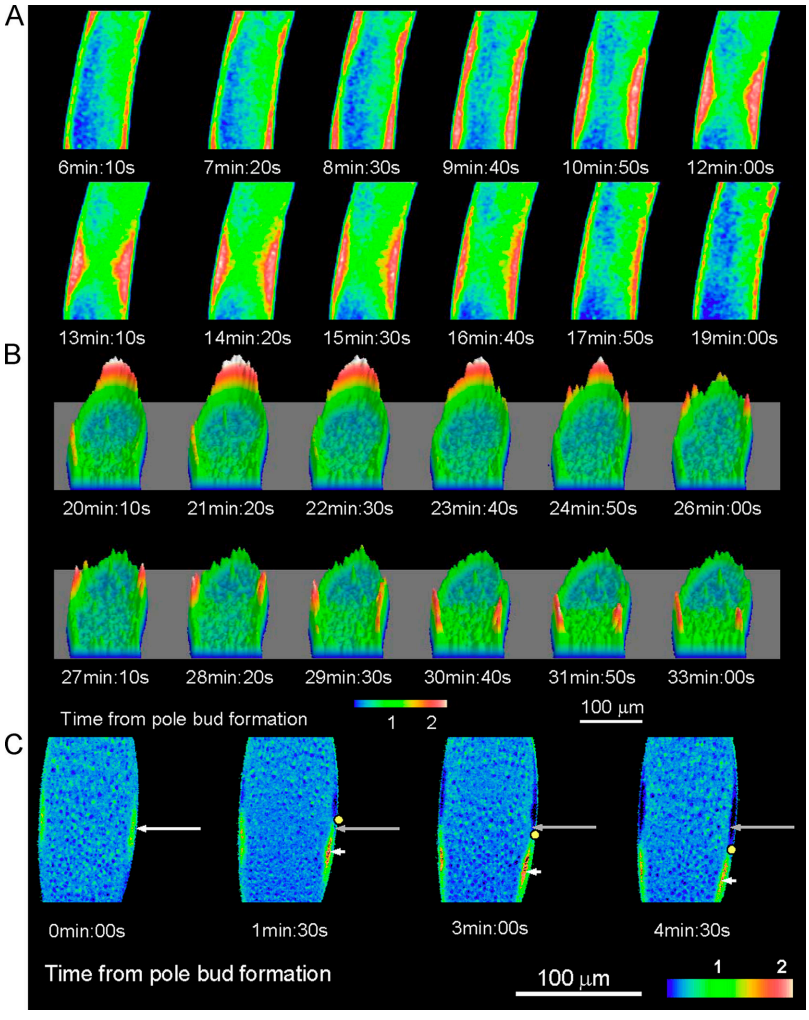

Figure 2. **The [Ca_i] increases are slow, periodic calcium waves that originate at both poles of the embryo and annihilate upon collision.** (A) The images display the CaGr/TMR confocal ratio of a section through an embryo in cycle 9. Slow calcium waves are seen moving toward the equator of the embryo from the poles and annihilating upon collision. The calcium wave speed in this cycle is ~0.4 μm/s (Table II). (B) Topographical representation of another slow calcium wave during cycle 10. The polar origin of the calcium wave is evident. The waves propagate cortically toward the equator of the embryo. (C) The slow calcium waves precede the wave of cortical contraction, which is seen as retraction of the plasma membrane away from the vitelline membrane. The images display CaGr/TMR confocal ratio images in a cycle 8 embryo. The slow cortical calcium wave moves vertically downwards away from the anterior pole, as indicated by the movement of arrowheads. The displacement of both the calcium wave and the cortical contraction are progressive. The arrowheads mark the region of highest calcium increase in each successive image, and the white arrow marks the starting position of the calcium increase at time = 0. The leading edge of the cortical contraction is marked by a yellow dot. Note that in this image, the embryo equator is beyond the bottom of the images and that the widest part of the image at the top is a property of the confocal section; it is not the embryo equator, which lies beyond the bottom of the images. Temperature is 18°C.

Table II. **Wave speeds during cycles 9–12**

	Cycle 9	Cycle 10	Cycle 11	Cycle 12
Embryo 1	0.47	0.37	0.36	0.29
Embryo 2	0.42	0.29	0.32	0.29
Embryo 3	0.46	0.46	0.42	0.25
Embryo 4	0.47	0.36	0.36	0.31
Embryo 5	0.43	0.43	0.40	0.31
Mean speed (v)	0.45 ± 0.02	0.38 ± 0.09	0.37 ± 0.05	0.29 ± 0.06
Cycle time (t; min)	9.3	11.0	11.3	14.4
Product (v × t)	4.15	4.18	4.18	4.18

Wave speeds in micrometers/second were calculated by measuring the time taken for the center of the wave to cover a fixed distance of 170 μm at either the anterior or posterior end (embryo 4 only) of an embryo. All measurements were made on embryos maintained at 18°C.

several microns deeper in the embryo (Fig. 1 C). The confocal images are a window into small areas of the embryo cortex.

This pattern of calcium oscillation, with maximum ratio increases in interphase, was seen in all 29 examined embryos. The oscillation remains in phase during the four nuclear cycles as cycle time lengthens with each nuclear division (Fig. 1 A). The increases were analyzed quantitatively in 17 embryos at various cell cycle stages. The data are shown in Table I. Mean $[Ca_i]$ in the trough during mitosis ranged from 0.10 ± 0.008 to 0.13 ± 0.018 μm across five nuclear cycles (Table I), and mean peak $[Ca_i]$ was 1.01 ± 0.305 μm in cycle 8, falling gradually to 0.35 ± 0.044 μm in cycle 13. Also note from the images of Fig. 1 that local $[Ca_i]$ continues to reach micromolar levels during each interphase in areas of the cortex surrounding the nuclei, even in later nuclear cycles. These observations indicate that calcium oscillations occur in fixed phase relation with the nuclear cycle in syncytial embryos and that $[Ca_i]$ is highest in interphase at the time of maximum cortical contraction (Foe et al., 1993).

Nuclear division cycles in syncytial embryos are sensitive to protein synthesis inhibitors (Boring et al., 1989); at limiting concentrations of cycloheximide, the division cycles are slowed but not blocked (Fig. 1 B). We injected cycloheximide (0.5 μg/ml at final concentration) to increase the duration of cycles 8–12 from 65.9 ± 1.2 to 79.1 ± 1.4 min (mean and SEM). Fig. 1 B shows that calcium oscillations continue in phase with the nuclear division cycle in cycloheximide-treated embryos, demonstrating a close mutual entrainment of calcium oscillations and the nuclear division cycle.

Calcium changes take the form of slow calcium waves that travel from pole to equator during each nuclear division cycle and precede the cortical contraction

When displayed at higher temporal resolution, the $[Ca_i]$ changes have a spatial substructure. Fig. 2 A shows two examples of the spatial pattern of $[Ca_i]$ increase. In the top panel, two $[Ca_i]$ waves are arriving from poles at the equator of the embryo and are annihilating there. In Fig. 2 B, the initiation of a calcium wave at the anterior pole is followed by progression of the wave toward the equator and out of the frame. Thus, the calcium signal shows the same behavior as mitotic waves, originating at both embryonic poles and moving toward the equator. Table II gives the mean wave velocity during syncytial division cycles from cycles 9–12. The wave speed slows with each cycle, decreasing from 0.45 to 0.29 μm/s. As the nuclear division cycle time slows, the wave becomes progressively slower; the product of wave speed and cycle time remains constant, which is a further indication of the entrainment of calcium wave and nuclear cycle. Fig. 2 C shows a single $[Ca_i]$ wave in a cycle 8 embryo before the nuclei have reached the cortex. As the wave progresses toward the equator, it is followed by a cortical constriction that represents a cortical contraction travelling at the same velocity. The constriction can be seen in the confocal section, as the movement of the plasma membrane away from the vitelline membrane creates a dye-free perivitelline space that appears black beneath the autofluorescent vitelline membrane. The time that elapsed between the leading edge of the calcium wave and the leading edge of the constriction is ∼90 s. We observed the association between wave and constriction in three of three embryos, suggesting that the $[Ca_i]$ increase causes the cortical contraction.

$InsP_3$-induced calcium release is required for mitotic progression

Cell cycle calcium signals in other early embryos are triggered by inositol trisphosphate ($InsP_3$; Ciapa et al., 1994; Muto et al., 1996; Groigno and Whitaker, 1998). *Drosophila* possesses a single insect-specific $InsP_3$ receptor isoform (Hasan and Rosbash, 1992; Yoshikawa et al., 1992). Deletion of the $InsP_3$ receptor arrests larval development at second instar, and embryos show defects in cell division and endoreplication (Acharya et al., 1997). Embryonic development to second instar also requires the $InsP_3$ receptor because no viable eggs or embryos were generated from germ line clones lacking the receptor (Acharya et al., 1997). Fig. 3 A shows that $InsP_3$ receptors are functional in early embryos; the microinjection of $InsP_3$ leads to calcium release. $[Ca_i]$ was measured using CaGr, and localization of the injected $InsP_3$ was determined by coinjection of rhodamine dextran with $InsP_3$. Although $InsP_3$ was injected into the body of the embryo, $[Ca_i]$ rose at the cortex predominantly, and there is also a cortical contraction response. This experiment shows that $InsP_3$-induced calcium release causes cortical contraction.

It was important to establish that $InsP_3$-triggered calcium signals are required for nuclear division in syncytial embryos. One way of specifically interfering with $InsP_3$ signaling is to use a dominant-negative approach and introduce $InsP_3$-binding proteins or binding domains into the cytoplasm (Takeuchi et al., 2000; Walker et al., 2002). We microinjected an $InsP_3$ sponge polypeptide consisting of the $InsP_3$-binding domain of type 1 $InsP_3$ receptor (Walker et al., 2002) into embryos at the start of cycle 11 and compared its effects with a control sponge in which two point substitutions had been made in the $InsP_3$-binding region to produce a polypeptide with no detectable $InsP_3$-binding affinity (Walker et al., 2002). Fig. 3 B (i) shows that 80% of embryos injected with the wild-type sponge arrested

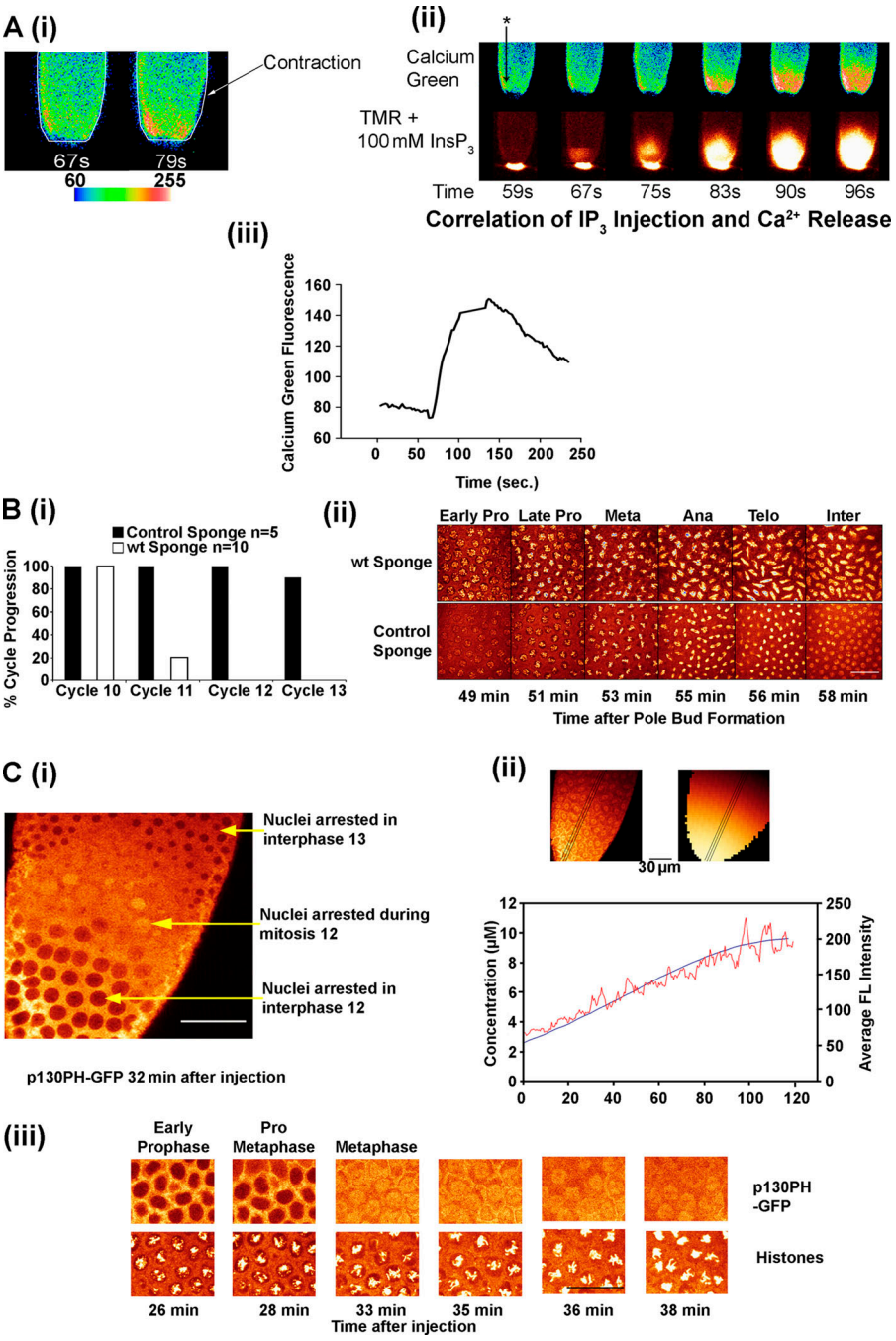

Figure 3. **Functional $InsP_3$ receptors in *Drosophila* embryos.** (A) To determine whether *Drosophila* embryos had functional $InsP_3$ calcium release channels, $InsP_3$ was injected into cycle 8 embryos. The site of injection is indicated by an asterisk. (i) Microinjection of $InsP_3$ (pipette concentration of 100 µM; final concentration of 200 nM) at 67 s increases $[Ca]_i$ and results in a cortical contraction in CaGr-injected embryos. The outline of the embryo is shown in white, and the contraction is seen as a retraction of the plasma membrane beneath the perivitelline envelope. (ii) $InsP_3$ was coinjected with TMR to verify the site of injection. The top row is comprised of CaGr confocal images, whereas the bottom row displays TMR confocal images. To verify that there was no spillover from the TMR signal into the CaGr recording channel, the perivitelline space was first loaded with TMR (first image: 59 s). $InsP_3$ microinjection causes a large calcium increase, indicating that functional $InsP_3$ receptors are present. The cortical contraction is visible in these images by 8–9 s after the injection of $InsP_3$. (iii) The time course of CaGr fluorescence increase in the embryo, corresponding to an increase in $[Ca_i]$. The embryo was in cycle 8. (B) Effects of wild-type and control (inactive) $InsP_3$ sponge. (i) Nuclear cycle progression fails after microinjection of the $InsP_3$ sponge during interphase of cycle 10 (20 mg/ml in pipette; 40 µg/ml in the embryo if uniformly distributed) but is unaffected by the mutated control sponge (20 mg/ml in pipette). (ii) Nuclear morphology visualized with fluorescein histones during mitosis of cycle 11 using the same microinjection protocol. With wild-type sponge, NEB, chromatin condensation, and metaphase plate formation occur normally, but anaphase onset is delayed, and chromosomes fail to separate. In contrast, embryos that were injected with the control sponge in parallel experiments have reformed normal nuclei in cycle 11; chromatin decondensation after mitosis occurs but is abnormal. (C) Effects of p130 $InsP_3$-binding protein that was injected into cycle 11 embryos as they entered interphase to produce a gradient of inhibitor. (i) Imaging microinjected GFP::p130 fluorescence is associated with cytoplasm and plasma membrane and with ER at interphase and enters the nucleus as NEB occurs. At the highest concentrations, nuclei arrest in interphase of the following cycle, cycle 12. At intermediate concentrations, nuclei arrest with condensed chromosomes in metaphase of cycle 12. At lowest concentrations, nuclei arrest in interphase of cycle 13. From the fluorescence distribution, note the concentration gradient of the inhibitor (injected at a pipette concentration of 30 mg/ml = 200 µM at anaphase of cycle 10, 32 min before the time of the image shown) from the bottom to top of the field. (ii) Calibration of concentration gradient (see Materials and methods). The experimental image and model show the distribution 15 min after microinjection. Lines across the images indicate the pixels that were sampled. FL, fluorescence. Numbers on x axis represent distance in pixels. (iii) Higher magnification of a separate experiment using an identical experimental protocol to show eventual chromatin decondensation after failed anaphase onset. Temperature is 18°C. In these experiments, the time of pole bud formation was not recorded. Bars, 30 µm.

their nuclear division within one cycle, whereas the remainder arrested in the next division cycle. A comparison of histone-tagged chromatin indicates that the embryos microinjected with wild-type sponge form normal metaphase figures but that anaphase failed to take place. The spindle and chromatin also elongated (some with the dumbell shape that is characteristic of anaphase bridges). Chromosomes failed to separate, decondensing to form the same number of nuclei as before (Fig. 3 B ii). Then, the nuclei rapidly sank from the field of view and could not be followed further but remained in a state of arrest for as long as they were visible in deep confocal sections (not depicted).

Because nuclei in the syncytial embryo are not separated by plasma membranes, the syncytial embryo offers the possibility of generating a gradient of inhibitor within the cytoplasm so that individual nuclei will experience different concentrations of inhibitor. GFP::p130 is a PLCδ orthologue that is catalytically

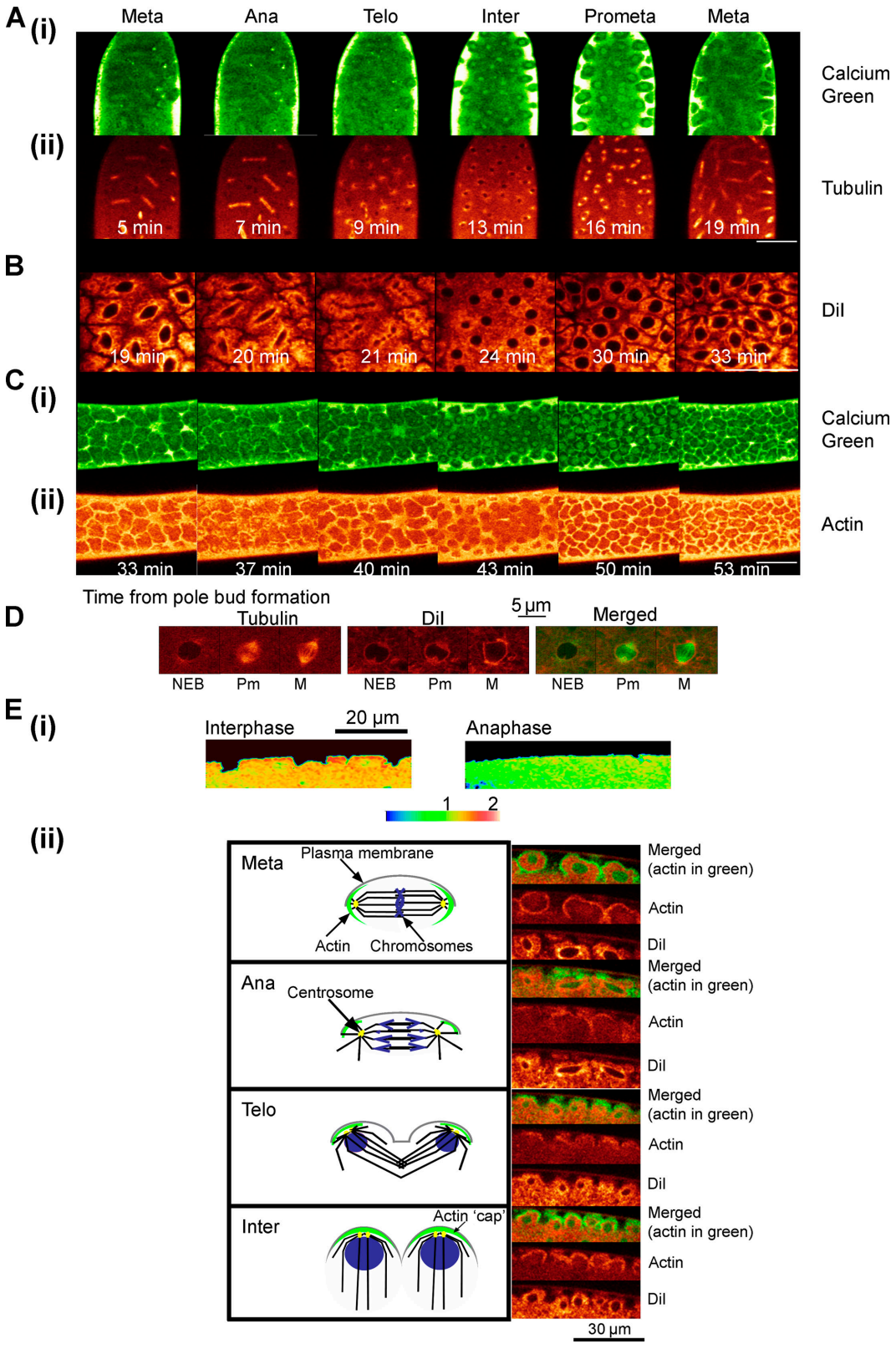

Figure 4. **Spatial correlation of cortical calcium signals, the cortical cytoskeleton, and ER after the arrival of nuclei at the cortex.** (A) Embryo coinjected with CaGr and rhodamine tubulin. (i) CaGr confocal images from metaphase of cycle 10 to metaphase of cycle 11. Increasing detector sensitivity in order to better detect the nuclear CaGr signal, which leads to saturation of the signal in the cortex. The $[Ca_i]$ increase during interphase is highest in the region surrounding the nuclei. (ii) Simultaneous rhodamine tubulin confocal images from the same sections that display the microtubule configuration and permit determination of the phase of the cell cycle during mitosis. Embryo is in cycle 9. (B) Confocal images revealing the distribution of the ER during mitosis in a different embryo. Embryos were injected with the lipophilic dye $DiIC_{18}$ to label the ER. During mitosis, the ER is concentrated around the mitotic spindle, at the poles during metaphase and anaphase, and at the midbody in telophase. Also note the ER-free interstices between spindles. During interphase, ER is absent from the nuclei, as might be expected, and is dispersed relative to mitosis. Embryo is in cycle 10. (C) Further embryos were coinjected with

inactive, binds $InsP_3$ with high affinity by virtue of its pleckstrin homology domain, and inhibits calcium signaling when overexpressed in cells or when added to permeabilized cells (Takeuchi et al., 2000). The GFP::p130 chimera was localized to plasma membrane and apparently to ER in interphase, entered the nucleus at prophase, and associated with the mitotic spindle (Fig. 3 C i). By microinjecting GFP::p130 at one pole of the embryo during early anaphase of cycle 11, we were able to generate a gradient of GFP::p130 of 2–10 μM, which was confirmed by the distribution of fluorescence (Fig. 3 C ii) that persisted for the course of the experiment. The outcome was striking. Nuclei that were exposed to 10 μM GFP::p130 arrested before nuclear envelope breakdown (NEB) in cycle 12. Nuclei that were exposed to intermediate concentrations continued through NEB of cycle 12 but arrested after mitosis entry and were unable to complete mitosis, whereas nuclei that were exposed to 2 μM progressed through mitosis of cycle 12 and arrested before mitosis in cycle 13. Simultaneous imaging of histone and GFP signals demonstrated that nuclei entered metaphase but failed to enter anaphase rapidly, just as we had found with the $InsP_3$ sponge (Fig. 3 C iii). Chromatin decondensation occurred in the arrested nuclei after a delay (Fig. 3 C iii) and elongated, and dumbell-shaped nuclei were also seen (not depicted), although this occurred a few minutes later than we had observed after the microinjection of $InsP_3$ sponge constructs. These observations demonstrate that $InsP_3$ signaling plays a role in mitosis entry at NEB as well as in mitosis exit in *Drosophila* embryos. In GFP::p130-injected embryos, the mitotic wave (the wave of NEB and anaphase onset) travelled in the opposite direction to that observed in controls (that is, from the farther embryonic pole), indicating that $InsP_3$ is involved in the initiation and propagation of the wave.

Heparin and Xestospongin C are agents that inhibit the interaction of $InsP_3$ with the $InsP_3$ receptor (Ghosh et al., 1988; Gafni et al., 1997). Embryos that were microinjected with either the inhibitor of $InsP_3$-induced calcium release, heparin (80 μg/ml gave half maximum inhibition; $n = 4$; Groigno and Whitaker, 1998), or Xestospongin C (10 mM of pipette concentration; $n = 6$; Hu et al., 1999) also showed a block in mitosis that was similar to what we observed with both the $InsP_3$ sponge and GFP::p130 (unpublished data). As far as is known, the $InsP_3$ receptor is the sole signaling target of $InsP_3$ in cells (for review see Fukuda and Mikoshiba, 1997; Mikoshiba, 1997).

These experiments demonstrate that $InsP_3$-triggered calcium release is a signal that is necessary for both entry into mitosis and for anaphase onset in syncytial *Drosophila* embryos, as it is in sea urchin embryos (Twigg et al., 1988a; Ciapa et al., 1994; Groigno and Whitaker, 1998).

Microdomains of elevated calcium that are separated by ER-rich low calcium domains are observed in cortical buds

Once nuclei reach the surface, it is possible to stage the nuclear cycle precisely. Fig. 4 shows the spatial distribution of the interphase $[Ca_i]$ increase from metaphase through interphase to metaphase of the next cycle, as seen in glancing tangential confocal sections (Fig. 1 C); this is compared with the disposition of mitotic spindles, ER, and actin. CaGr fluorescence (Fig. 4 A, i and ii) indicates that the major $[Ca_i]$ increase occurs in interphase in a cortical region surrounding the nuclei but is separated from interphase nuclei by a region of low calcium concentration. As nuclei enter mitosis, the cortical $[Ca_i]$ levels fall overall, and the signal becomes confined to narrower regions surrounding the mitotic spindle. $[Ca_i]$ in the nucleus and mitotic spindle appears higher than in the circumnuclear region but much lower than in the cortical region. These images cannot be compared directly to those of Fig. 1, as ratiometric methods cannot be used when simultaneously measuring rhodamine-tagged cytoskeletal components. Moreover, the increased detection sensitivity that is required to visualize CaGr fluorescence in the nucleus and spindle leads to saturation of the cortical CaGr signal because of the limited dynamic range of the confocal microscope.

Fig. 4 B shows, in a separate experiment, changes in ER distribution during the nuclear division cycle, which was visualized using DiI, a lipophilic carbocyanine dye that labels ER and other elements of the ER/Golgi/endosome system (Terasaki and Jaffe, 1991). The pattern of DiI fluorescence is identical to that reported for an ER-localized GFP-tagged protein in early *Drosophila* embryos (Bobinnec et al., 2003). The ER extends diffusely into the space between nuclei during interphase and is markedly concentrated immediately around the mitotic spindle during mitosis (Fig. 4 D). It is excluded from the spindle until late telophase, when ER invades the spindle in the region of the midbody. The pattern of distribution of cortical ER (Fig. 4 B) is linked to the pattern of $[Ca_i]$ increase, with $[Ca_i]$ being highest in the interstices between ER accumulation around the nuclei

rhodamine-labeled actin and CaGr to determine the spatial relation between actin and $[Ca]_i$. (i) Confocal images that display the pattern of calcium increase from mitosis to mitosis. (ii) The distribution of actin in the same confocal sections. The pattern of $[Ca]_i$ increase follows the pattern of actin distribution closely throughout the nuclear cycle. Embryo is in cycle 11. Bars, 50 μm. (D) Simultaneous imaging of ER (DiI fluorescence) and the mitotic spindle (fluorescein tubulin fluorescence). The images show that the ER surrounds the spindle as the nucleus enters mitosis. NEB, nuclear envelope breakdown; Pm, prometaphase; M, metaphase. (E) To determine the spatial relationships between the ER, actin, and $[Ca_i]$, embryos were coinjected with fluorescein-labeled actin and $DiIC_{18}$ and were compared with other embryos that were injected with CaGr/TMR ratios in confocal z-sections. (i) Confocal ratiometric images normal to the surface of the embryo compare the cortical $[Ca_i]$ levels during interphase, when the actin caps are present in cortical buds, with those at anaphase. The $[Ca]_i$ increase occurs through this thickness of cortex in interphase but is very prominent just beneath the plasmalemma within the cortical bud. During anaphase, cortical buds are absent and $[Ca_i]$ levels are both lower and more uniform beneath the cortex. (ii) Cartoons displaying the distribution of actin, microtubules, and chromosomes during metaphase, anaphase, telophase, and interphase accompanied by images of actin and ER in cortical buds in sections normal to the cortex (z sections) as mitosis progresses. Embryos were coinjected with fluorescein-actin and $DiIC_{16}$ to visualize the cortical actin and ER during mitosis. Confocal merged images reveal that the actin (green) and ER (red) are in close apposition but do not overlap significantly. ER was found below the actin cap. A comparison with (i) indicates that $[Ca_i]$ is highest in the region of the actin cap. ER wraps around the nucleus and mitotic spindle. Results shown are representative of data from at least three embryos in separate experiments. Temperature is 18°C.

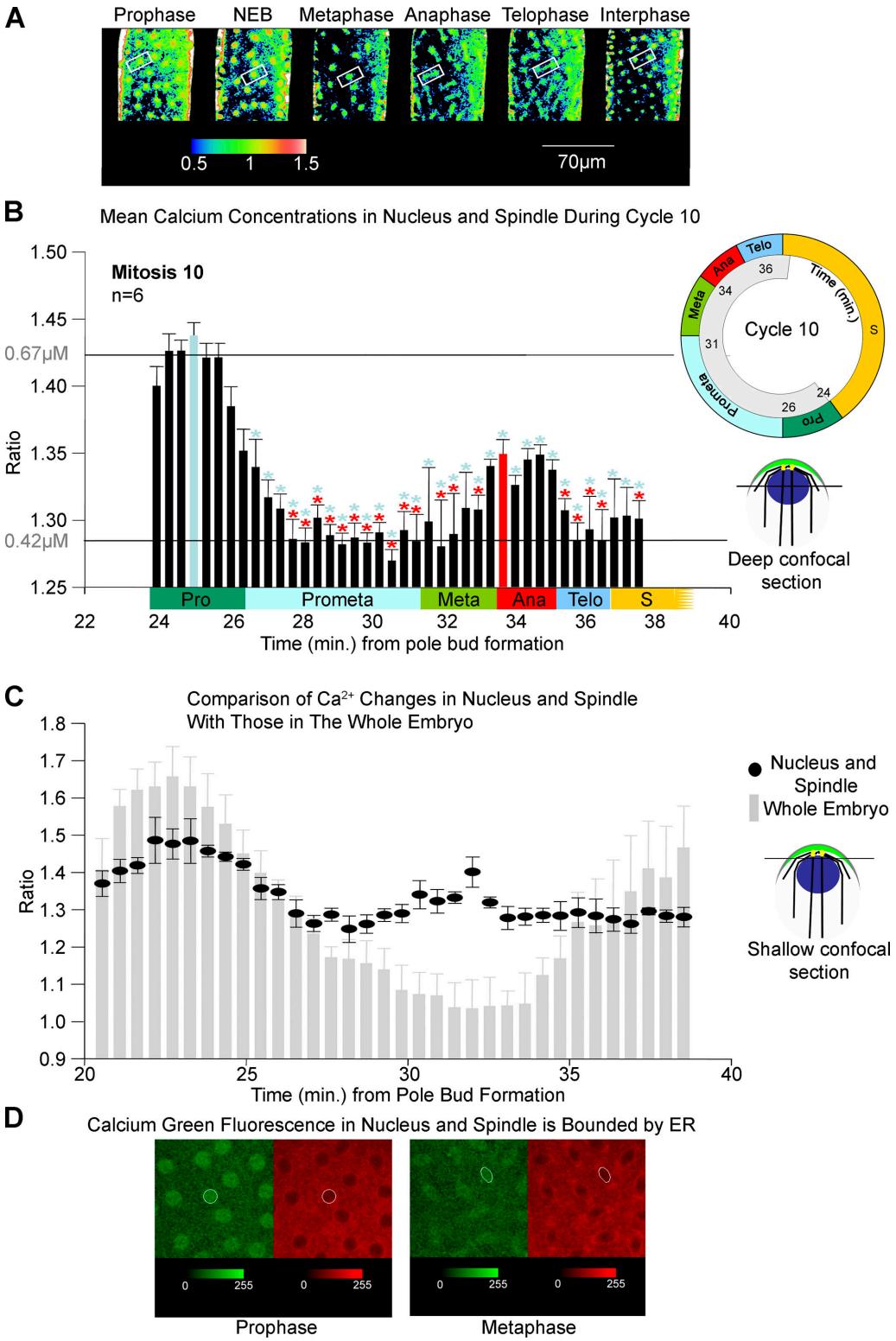

Figure 5. **Calcium increases in the nucleus and spindle microdomains during mitosis.** (A) Confocal ratio images of embryos that were injected with CaGr/TMR during cycle 10. Calcium dynamics in and around an individual nucleus were measured in the region of interest that is displayed on the images (white boxes). Note that individual nuclei move tens of microns as the nuclear division cycle progresses. In this region of interest, calcium increases during interphase before NEB (NEB occurs at the prophase/prometaphase boundary) and again during metaphase/anaphase. The time between images varies (see inset schematic for the timing of this cell cycle relative to pole cell formation). Also note that in order to visualize the nuclei in quasi-equatorial section, these confocal sections are deeper than those of Figs. 1–4 (also shown schematically) so that the nucleus-associated calcium changes are more evident than in previous figures. (B) Quantitative analysis of six similar experiments. Data from the regions of interest are expressed as the ratio versus time. The light blue column indicates the peak interphase calcium signal. This column is significantly different from all columns marked with a light blue star ($P < 0.05$). The red column represents the peak anaphase calcium signal. This calcium increase is significantly different from all columns marked with a red star ($P < 0.05$). S, S phase. (C) Comparison of [Ca_i] in the nucleus and mitotic spindle microdomain (circles) with [Ca_i] in the embryo section as a whole (bars)

and spindles (Fig. 4, A i and C i). Fig. 4 C (ii) shows the pattern of distribution of cortical actin during the nuclear division cycle, which was visualized using rhodamine-actin simultaneously with CaGr (Fig. 3 C i). There is a close correspondence between the distribution of actin and regions of highest $[Ca_i]$ increase. During mitosis, actin is localized to the interstices between ER that were noted above. The ER appears to isolate the nucleus and mitotic spindle from these regions of highest $[Ca_i]$ as nuclei enter and progress through mitosis (Fig. 4 D).

The interphase $[Ca_i]$ increase occurs at the very periphery of cortical buds that surround the interphase nuclei (Fig. 4 E i). Cortical mitotic spindles are anchored by actin caps that surround each nucleus in interphase (Fig. 4 E ii, cartoon; Sullivan and Theurkauf, 1995; Foe et al., 2000). The actin caps are pushed further apart as the spindles extend at anaphase. In late telophase, the actin wraps around the reforming interphase nucleus to give twice as many actin caps as were present before nuclear division (Fig. 4 E ii). Nuclei, therefore, occupy a greater area of the cortex in mitosis compared with interphase, which gives rise to substantial oscillatory translation of nuclei in the plane of the cortex as the mitotic wave progresses along the embryo (Zalokar and Erk, 1976). When localization of the interphase $[Ca_i]$ increase, actin, and ER distribution are compared in confocal sections normal to the surface (Fig. 4 E, i and ii), it is evident that the $[Ca_i]$ increase occurs throughout the cortex in each cap but is markedly higher in the regions of highest actin concentration.

As predicted, the halo of ER that surrounds the nucleus and mitotic spindle appears to separate two distinct calcium microdomains: a region of high calcium in the subcortex, which is associated with actin and contraction in interphase, and a region of lower nuclear calcium. Calcium concentrations are lowest where the ER is most dense.

$[Ca_i]$ increases occur in the nucleus and mitotic spindle microdomains at both prophase and anaphase

To confirm that calcium increases occurred at prophase and anaphase, as would be predicted from observations in sea urchin embryos (Ciapa et al., 1994; Wilding et al., 1996; Groigno and Whitaker, 1998), we used ratiometric calcium imaging of single nuclei. We screened for $[Ca_i]$ increases by tracking the $[Ca_i]$ changes in and around individual nuclei during a nuclear cycle in cycle 10 in six different embryos (Fig. 5, A and B). Note that individual nuclei travel quite large distances along the cortex of the embryo as nuclear divisions progress (Zalokar and Erk, 1976). We chose a level of confocal section that was deeper in the buds than that shown in Fig. 4 (level 2; Fig. 5 D) in order to image nuclear calcium; at this level of confocal section, the cortical increase in $[Ca_i]$ can be seen only at the very periphery of the deep section through the embryo (Fig. 5 A). Fig. 5 demonstrates that an increase in nuclear $[Ca_i]$ occurs at a time that coincides with the aforementioned larger global cortical interphase $[Ca_i]$ increase, and it falls as nuclei enter prometaphase. Peak $[Ca_i]$ was less than that observed in the whole embryo (Fig. 5 B). In addition, we detected a second $[Ca_i]$ increase in the mitotic spindle at around the time of anaphase onset (Fig. 5 B). When we tracked nuclei using ratiometric imaging with the 70-kD form of CaGr, which is excluded from the nucleus during interphase, we observed a local $[Ca_i]$ increase in the spindle at anaphase. However, the NEB-associated signal was absent (unpublished data), confirming that the local $[Ca_i]$ increase at prophase occurred within the nucleus.

To make a direct comparison between cortical and nuclear calcium concentrations in individual cortical buds, we used ratiometric imaging with confocal sections at the shallower level used in Fig. 4 to enable us to visualize both cortical and nuclear calcium simultaneously (level 1; Fig. 5 D). We found the calcium concentration in the nuclear microdomain to be significantly lower than cortical calcium at prophase and significantly higher than cortical calcium levels at anaphase onset (Fig. 5 C). These experiments also confirmed that the peak of nuclear calcium at prophase coincided with the peak of cortical calcium concentration. Simultaneous imaging of $[Ca_i]$ and ER at metaphase just before anaphase onset showed that $[Ca_i]$ in the spindle was confined to the space enclosed by ER (Fig. 5 E).

These data demonstrate the existence of nuclear microdomains of calcium concentration that act as triggers for mitosis entry and exit.

Discussion

The interphase $[Ca_i]$ signal is linked to contraction, the actin cytoskeleton, and the cortical ER

The interphase $[Ca_i]$ increase occurs very close to the surface of the embryo in the space between the nucleus and its cap that contains both actin and ER. High $[Ca_i]$ correlates with the phase of cortical contraction that is associated with interphase nuclei. Alternating bands of contraction/relaxation pass along the embryo as the calcium signal progresses, giving rise to large oscillations in nuclear position that were observed in the cortex, which are referred to as yolk contractions (Foe et al., 1993) and are inhibited by cytochalasins (Hatanaka and Odada, 1991). Progressive, slow calcium waves have been observed in the cleavage furrows of early fish embryos (Webb and Nuccitelli, 1985; Fluck et al., 1991; Chang and Meng, 1995; Webb et al., 1997; Lee et al., 2003; Webb and Miller, 2003), and $[Ca_i]$ increases have also been recorded in frog embryos (Steinhardt

during cycle 11 in five embryos at level 1, which is shown in D. The interphase peak of nuclear $[Ca_i]$ coincides with the cortical interphase $[Ca_i]$ peak but is of lower magnitude. Note the shallow confocal section that is illustrated schematically and is similar to that in Figs. 1–4. Temperature is 18°C. Error bars represent SEM. (D) Simultaneous imaging of $[Ca_i]$ using CaGr and of ER using $DiIC_{18}$. Two pairs of images from an image series are shown, illustrating prophase and metaphase just before anaphase onset in cycle 10. Green, CaGr; red, $DiIC_{18}$. White encircled areas are of equal size and position. These images show the spatial relationship between CaGr fluorescence and ER but are only indicative of $[Ca_i]$, as they are nonratiometric. Temperature is 18°C.

et al., 1974; Miller et al., 1993; Snow and Nuccitelli, 1993; Muto and Mikoshiba, 1998). A calcium signal at cytokinesis has also been shown to be essential for the insertion of new membrane into the cleavage furrow in the sea urchin embryo (Shuster and Burgess, 2002). During pseudocleavage in syncytial *Drosophila* embryos, membrane addition from endosomes is essential for actin recruitment and furrow elongation (Riggs et al., 2003). Calcium signals have been found to be associated with cortical contraction in ascidian and fish embryos (Roegiers et al., 1995; Leung et al., 1998).

$InsP_3$ and the $InsP_3$ receptor are essential for nuclear division

We determined that $InsP_3$ receptors were functional in early embryos by eliciting calcium release in response to $InsP_3$ injection. A genetic approach to determine the importance of $InsP_3$ signaling during rapid syncytial nuclear divisions of the *Drosophila* embryo does not easily present itself. In fact, despite the ubiquity and importance of calcium signaling (Berridge et al., 2000), very few genetic disorders that are caused by defects in calcium-signaling components have been identified; the strong assumption is that an overwhelming majority of genetic calcium signaling defects are embryonic lethals (Rizzuto and Pozzan, 2003). Instead, we microinjected constructs that have been shown to chelate $InsP_3$. We used a GFP-tagged $InsP_3$-binding protein to determine the cytoplasmic concentration of injected proteins. We determined the inhibitory concentration that blocks both NEB and anaphase onset to be 2–10 μM, which are concentrations comparable with those previously observed to block $InsP_3$-mediated events (Takeuchi et al., 2000) and are similar to those observed with an $InsP_3$ sponge (Uchiyama et al., 2002). Thus, $InsP_3$ signaling leading to calcium transients is essential for NEB and anaphase onset, as it is in early sea urchin embryos (Poenie et al., 1985; Steinhardt and Alderton, 1988; Twigg et al., 1988b; Ciapa et al., 1994; Wilding et al., 1996; Groigno and Whitaker, 1998). As observed in the sea urchin embryo (Groigno and Whitaker, 1998), the block to anaphase onset was characterized by absence of chromatin disjunction, but spindle elongation and chromatin decondensation did occur, often with a delay. The ER isolates the nucleus during mitosis and generates local nuclear calcium signals via $InsP_3$.

Cell cycle calcium signals that govern mitosis are not prominent in syncytial *Drosophila* embryos. We show that this is because the ER generates calcium-signaling microdomains within the cortical bud: one beneath the plasma membrane of the cortical buds and the other within the nucleus and mitotic spindle. There is a real possibility that the very different molecular environments are, in part, responsible for the different fluorescence signals that we measured in these different microdomains. However, at metaphase, the calcium concentrations that are reported by fluorescence reporters are uncorrelated, implying that calcium rises in only the spindle microdomain.

Although it has been clear for some time that ER associates with the nucleus and spindle (Terasaki and Jaffe, 1991), this has been interpreted as a mechanism to ensure proportionate inheritance of ER when cells divide (Barr, 2002). In this study, we demonstrate an additional, essential, and novel function—that of maintaining distinct calcium microdomains during cell division. Nuclear calcium has also been shown in some cell types to be regulated differentially to cytoplasmic calcium (Badminton et al., 1998; MacDonald, 1998), but this is thought to be a result of the properties of the nuclear envelope rather than of an accumulation of ER around the nucleus. Although it was originally proposed that a nuclear envelope persisted throughout mitosis as a spindle envelope during syncytial nuclear divisions (Harel et al., 1989), it is now clear that the nucleus becomes permeable to high molecular weight molecules early in prophase (that is, at the same time as in other cells) but that nuclear lamins persist until metaphase, disappearing before anaphase onset (Paddy et al., 1996). Thus, the nuclear envelope does not exist during mitosis to provide a diffusion barrier that would allow the mechanisms regulating calcium in intact nuclei to operate. On the other hand, the persistence of nuclear lamins may explain why the ER remains outside the spindle until late anaphase in syncytial embryos.

We show that it is possible to apply cell physiology methods to early *Drosophila* embryos to study calcium signaling. Our data clearly demonstrate for the first time in a protostome embryo that maneuvers designed to prevent calcium signals arrest the nuclear division cycle and that calcium signals are responsible for the waves of mitosis observed in syncytial *Drosophila* embryos. We also show for the first time that the nucleus and spindle exist within a calcium-signaling microdomain and that calcium increases that are necessary for progress through mitosis are small and localized. This has been possible because ER is excluded from the *Drosophila* spindle during mitosis. In other embryos and in mammalian somatic cells, ER is an intimate spindle component. Signals that are local to the spindle are less readily detected, perhaps explaining why calcium signals are not always observed during mitosis in some cell types.

Materials and methods

Preparation of embryos for microinjection

Drosophila embryos (strained with Oregon R) were used for all presented experiments. Flies were kept at RT in plastic bottles containing a solid food base (Elgin and Miller, 1980) with breathable stoppers. Optimum egg laying occurred 21 d after egg deposition. The adult flies were transferred to a fresh glass bottle containing a 5 × 10-cm strip of chromatography paper (3 MM; Whatman) to provide a place for the flies to rest and to decrease humidity. The bottle was capped with a 2.5% agar plate (small petri dishes fit the bottle necks) that was inverted and left for 30 min. The first collection was discarded, and subsequent collections were used experimentally. Adhesive tape (magic 3M; Scotch) was affixed to one side of a 22 × 64-mm coverslip by double-sided tape. Glue was prepared by dissolving the adhesive of Scotch tape in heptane, and the glue–heptane solution was pipetted onto the center of the coverslip and allowed to dry. Embryos were placed on the adhesive-coated coverslip. The coverslip supporting the embryos was transferred to a large petri dish containing silica gel crystals. The embryos were desiccated for 10 min (causing the loss of ~5% cell volume) and covered with mineral oil during injection and imaging (halocarbon oil; 50% halocarbon 27 and 50% halocarbon 700; Sigma-Aldrich) to prevent further desiccation. Any embryos that developed wrinkles during desiccation were discarded. The embryos were injected immediately after desiccation.

Chemicals

5,5′dibromoBAPTA (tetrapotassium salt) and fluorescent dyes were purchased from Invitrogen. Cycloheximide and Xestospongin C were purchased from Calbiochem. The majority of all other chemicals were purchased from Sigma-Aldrich.

Microinjection

Drawn borosilicate glass micropipettes (GC150F-10; Clarke Electromedical) were loaded with injection solution and advanced toward immobilized *Drosophila* embryos by using an Eppendorf microinjection system. All fluorescent probes for microinjection were dissolved in injection solution (Ashburner et al., 2005) except Xestospongin C (Gafni et al., 1997), which was dissolved in DMSO for microinjection. The embryos were injected using gas pressure (pneumatic picopump; World Precision Instruments, Inc.). Cytoplasmic concentrations were calibrated by first measuring the size of droplets that were injected into the oil before injection into the embryo. Embryos are ~470 × 160 μm but can vary in length and diameter considerably. The approximate volume of an embryo is 6.5 nl, which was calculated by considering the volume of an ellipsoid of the above dimensions. The volume of liquids that were injected into the embryo was estimated by measuring the diameter of a droplet injected under mineral oil. This was 28 μm, giving an injected volume of 12 pl (i.e., ~1:500 embryo vol). The concentration gradient of injected fluorescent protein was calibrated by diffusion modeling (http://www.nrcam.uchc.edu/) to calculate the intraembryonic gradient of protein 15 min after microinjection of a 12-pl vol of 200 μM GFP::p130. The fitted diffusion constant was 3 $\mu m/s^{-1}$. The gradient remained stable from 10 min after microinjection and for the rest of the time course of the experiment.

Fluorescence measurements

An inverted confocal microscope (model DMIRBE; Leica) and either 20× PL Fluotar NA 0.5 or 40× PL Apo NA 1.25 objectives (Leica) were used for all described experiments. The light source was an argon–krypton laser with two excitation beams, which are available at 488 and 568 nm. Calcium measurements were performed using two fluorescent dyes: one was calcium sensitive (10 kD CaGr) and the other was calcium insensitive (10 kD tetramethylrhodamine dextran [TMR]). CaGr was excited at 488 nm, and TMR was excited at 568 nm with a dichroic mirror at 580 nm. Emission filters were a 530 ± 30 nm FITC bandpass and a 590 nm longpass. Images were acquired by using Scanware 5.1 software (Leica). Ratio images were performed for each image pair after background subtraction. All image processing was performed on a silicon graphics computer using IDL software (Research Systems International, Ltd.), and background-subtracted pixel values were displayed in pseudocolor using monochrome or rainbow look-up tables. Images were merged by using either Adobe Photoshop or Metamorph software. All experiments were performed at 18°C.

The ER was labeled with 1,1′-dioctadecyl-3,3,3′,3′-tetramethylindocarbocyanine perchlorate ($DiIC_{18}$) to determine its distribution (molecular mass of 933.8 D; Invitrogen). This dye was also used to visualize the location of the ER throughout early development of the *Drosophila* embryo. DiI was made up to a saturated concentration in soybean oil and was microinjected into cells in an oil droplet. The dye diffused along the continuous ER. DiI was excited by the 568-nm line of the argon–krypton laser. The maximum emission wavelength of DiI is 575 nm. Excitation and emission wavelengths were separated by a DD488/568-nm beamsplitter. The emission light was passed back through the beamsplitter and through a barrier filter before entering the photomultiplier tube.

To monitor microtubule dynamics, 10 mg/ml rhodamine-labeled tubulin (Cytoskeleton, Inc.) was microinjected into the embryos (dye/protein heterodimer stochiometry of 1.0). Identical settings that were used to record TMR fluorescence were used to measure rhodamine tubulin fluorescence.

5 mg/ml rhodamine-labeled histone H1 was prepared (Harlow and Lane, 1999) and injected into embryos to monitor the chromatin configuration to permit precise scoring of the stages of mitosis (dye protein stochiometry of 1.0). Identical settings that were used to record TMR fluorescence was used to measure histone H1 fluorescence.

To measure actin dynamics, we used rhodamine or fluorescein-conjugated rabbit nonmuscle actin (10 mg/ml dye/actin; labeling stochiometry of 1:1; Cytoskeleton, Inc.).

Calibration of ratiometric calcium signals

The fluorescence intensity of CaGr1 (made up in injection buffer) was determined in the absence of Ca^{2+} and in the presence of saturating Ca^{2+}. The fluorescence enhancement α (fluorescence in saturating Ca^{2+}/fluorescence in the absence of Ca^{2+}) was found to be 2.55. Single wavelength calcium dyes cannot readily be calibrated absolutely in *Drosophila* embryos, so calcium concentrations were estimated by using the following approach (Isenberg et al., 1996):

$$[Ca^{2+}{}_i] = \frac{K_D[F(\alpha[Ca^{2+}]_r/K_D + 1) - F_r(1 + [Ca^{2+}]_r/K_D)]}{\alpha F_r(1 + [Ca^{2+}]_r/K_D) - F(\alpha[Ca^{2+}]_r/K_D + 1)}$$

where F_r is the fluorescence at "resting" calcium ($[Ca^{2+}]_r$), which we have taken to be 100 nM during mitosis of cycle 10. Gillot and Whitaker (1994) calculated the K_D for CaGr1 (when coupled to a 10-kD dextran) to be 2 μM in the sea urchin egg. The K_D for CaGr1 in the *Drosophila* embryo is likely to be lower as a result of the ionic strength of the *Drosophila* embryo's cytoplasm, which is intermediate between that of marine and vertebrate embryos (Van der Meer and Jaffe, 1983). Accordingly, the calcium concentration in Fig. 1 has been calibrated by using two values for the K_D of 1 and 2 μM, respectively.

Protein expression

The GFP::p130 domain construct (Takeuchi et al., 2000) was obtained from M. Katan (Imperial College, London, UK) and was cloned into the expression vector pGEX-6-p1 (GE Healthcare) as follows: GFP::p130 was cut with HindIII, and the 1.3-kb fragment was cloned into pBC SK (+) digested with HindIII. The 1.3-kb EcoRI-SalI fragment was then cloned in frame into pGEX-6-p1 that was cut with the same enzymes. Protein expression and purification were performed in accordance with the supplied manual (GE Healthcare). $InsP_3$ sponge constructs (wild-type and control sponge) were subcloned from the supplied pGEM-T vector (Howard Baylis, University of Cambridge, Cambridge, UK; Walker et al., 2002) into the expression vector pCal-n (Stratagene). The NcoI-SalI fragment was subcloned in frame into pCal-n that was digested with the same enzymes. Expression and purification was performed in accordance with the supplied manual.

We thank Pierre Leopold for his early interest in this project, Maureen Sinclair and Trevor Jowett for help with *Drosophila*, Howard Baylis and Matilda Katan for $InsP_3$-binding protein constructs, and Michael Aitchison for help with preparation of the figures.

We also thank the Biotechnology and Biological Sciences Research Council and Wellcome Trust for financial support.

Submitted: 24 March 2005
Accepted: 1 September 2005

References

Acharya, J.K., K. Jalink, R.W. Hardy, V. Hartstein, and C.S. Zucker. 1997. $InsP_3$ receptor is essential for growth and differentiation but not for vision in *Drosophila*. *Neuron.* 18:881–887.

Ashburner, M., G.G. Kent, and R.S. Hawley. 2005. *Drosophila*: A Laboratory Handbook. Cold Spring Harbor Laboratory Press, Cold Spring Harbor, NY. 1409 pp.

Badminton, M.N., J.M. Kendall, C.M. Rembold, and A.K. Campbell. 1998. Current evidence suggests independent regulation of nuclear calcium. *Cell Calcium.* 23:79–86.

Baitinger, C., J. Alderton, M. Poenie, H. Schulman, and R.A. Steinhardt. 1990. Multifunctional Ca^{2+}/calmodulin-dependent protein kinase is necessary for nuclear envelope breakdown. *J. Cell Biol.* 111:1763–1773.

Barr, F.A. 2002. Inheritance of the endoplasmic reticulum and Golgi apparatus. *Curr. Opin. Cell Biol.* 14:496–499.

Berridge, M.J., P. Lipp, and M.D. Bootman. 2000. The versatility and universality of calcium signalling. *Nat. Rev. Mol. Cell Biol.* 1:11–21.

Bobinnec, Y., C. Marcaillou, X. Morin, and A. Debec. 2003. Dynamics of the endoplasmic reticulum during early development of *Drosophila melanogaster*. *Cell Motil. Cytoskeleton.* 54:217–225.

Boring, L.F., B. Sinervo, and G. Schubiger. 1989. Experimental phenocopy of a minute maternal effect mutation alters blastoderm determination in embryos of *Drosophila melanogaster*. *Dev. Biol.* 132:343–354.

Chang, D.C., and C.L. Meng. 1995. A localized elevation of cytosolic-free calcium is associated with cytokinesis in the zebrafish embryo. *J. Cell Biol.* 131:1539–1545.

Ciapa, B., D. Pesando, M. Wilding, and M. Whitaker. 1994. Cell-cycle calcium transients driven by cyclic changes in inositol trisphosphate levels. *Nature.* 368:875–878.

Creton, R., J.A. Kreiling, and L.F. Jaffe. 2000. Presence and roles of calcium gradients along the dorsal-ventral axis in *Drosophila* embryos. *Dev. Biol.* 217:375–385.

Edgar, B.A., and C.F. Lehner. 1996. Developmental control of cell cycle regulators: A fly's perspective. *Science.* 274:1646–1652.

Elgin, S., and M.M. Miller. 1980. Mass rearing of flies and mass production and harvesting of embryos. *In* The Genetics and Biology of *Drosophila*. M. Ashburner and T.R.F. Wright, editors. Academic Press, NY. 112–121.

Evans, T., E.T. Rosenthal, J. Youngblom, D. Distel, and T. Hunt. 1983. Cyclin:

a protein specified by maternal mRNA in sea urchin eggs that is destroyed at each cleavage division. *Cell.* 33:389–396.

Fluck, R.A., A.L. Miller, and L.F. Jaffe. 1991. Slow calcium waves accompany cytokinesis in Medaka fish eggs. *J. Cell Biol.* 115:1259–1265.

Foe, V.E., and B.M. Alberts. 1983. Studies of nuclear and cytoplasmic behaviour during the five mitotic cycles that precede gastrulation in *Drosophila* embryogenesis. *J. Cell Sci.* 61:31–70.

Foe, V.E., G.M. Odell, and B.A. Edgar. 1993. Mitosis and morphogenesis in the *Drosophila* embryo: point and counterpoint. *In* The Development of *Drosophila melanogaster*. A. Martinez Arias, editor. Cold Spring Harbor Laboratory Press, Cold Spring Harbor, NY. 149–300.

Foe, V.E., C.M. Field, and G.M. Odell. 2000. Microtubules and mitotic cycle phase modulate spatiotemporal distributions of F-actin and myosin II in *Drosophila* syncytial embryos. *Development.* 127:1767–1787.

Fukuda, M., and K. Mikoshiba. 1997. The function of inositol high polyphosphate binding proteins. *BioEssays.* 19:593–603.

Gafni, J., J.A. Munsch, T.H. Lam, M.C. Catlin, L.G. Costa, T.F. Molinski, and I.N. Pessah. 1997. Xestospongins: potent membrane permeable blockers of the inositol 1,4,5-trisphosphate receptor. *Neuron.* 19:723–733.

Gautier, J., C. Norbury, M. Lohka, P. Nurse, and J. Maller. 1988. Purified maturation-promoting factor contains the product of a *Xenopus* homolog of the fission yeast cell cycle control gene cdc^{2+}. *Cell.* 54:433–439.

Ghosh, T.K., P.S. Eis, J.M. Mullaney, C.L. Ebert, and D.L. Gill. 1988. Competitive, reversible, and potent antagonism of inositol 1,4,5-trisphosphate-activated calcium release by heparin. *J. Biol. Chem.* 263:11075–11079.

Gillot, I., and M. Whitaker. 1994. Calcium signals in and around the nucleus in sea urchin eggs. *Cell Calcium.* 16:269–278.

Glover, D.M., S. Llamazares, C. Girdham, G. Maldanado Codina, A. Moreira, A. Tavares, C.E. Sunkel, and C. Gonzalez. 1991. Cyclical changes in the subcellular distribution of proteins essential for mitosis during embryogenesis in *Drosophila*. *Cold Spring Harb. Symp. Quant. Biol.* 56:709–717.

Glover, D.M., M. Leibowitz, D.A. McLean, and H. Parry. 1995. Mutations in aurora prevent centrosome separation leading to the formation of monopolar spindles. *Cell.* 81:95–105.

Gonzalez, C., L. Alphey, and D. Glover. 1994. Cell cycle genes of *Drosophila*. *Adv. Genet.* 31:79–138.

Groigno, L., and M. Whitaker. 1998. An anaphase calcium signal controls chromosome disjunction in early sea urchin embryos. *Cell.* 92:193–204.

Harel, A., E. Zlotkin, E.S. Nainudel, N. Feinstein, P.A. Fisher, and Y. Gruenbaum. 1989. Persistence of major nuclear envelope antigens in an envelope-like structure during mitosis in *Drosophila melanogaster* embryos. *J. Cell Sci.* 94:463–470.

Harlow, E., and D. Lane. 1999. Using Antibodies: A Laboratory Manual. Cold Spring Harbor Laboratory Press, Cold Spring Harbor, NY. 495 pp.

Harris, P. 1975. The role of membranes in the organization of the mitotic apparatus. *Exp. Cell Res.* 94:409–425.

Hasan, G., and M. Rosbash. 1992. *Drosophila* homologues of two mammalian intracellular Ca^{2+}-release channels: identification and expression patterns of the inositol 1,4,5-trisphosphate and ryanodine receptor genes. *Development.* 116:967–975.

Hatanaka, K., and M. Odada. 1991. Retarded nuclear migration in *Drosophila* embryos with aberrant F-actin reorganization caused by maternal mutations and by cytochalasin treatment. *Development.* 111:909–920.

Hu, Q., S. Deshpande, K. Irani, and R.C. Ziegelstein. 1999. $[Ca^{(2+)}]$(i) oscillation frequency regulates agonist-stimulated NF-kappaB transcriptional activity. *J. Biol. Chem.* 274:33995–33998.

Isenberg, G., E.F. Etter, M.F. Wendt-Gallitelli, A. Schiefer, W.A. Carrington, R.A. Tuft, and F.S. Fay. 1996. Intrasarcomere $[Ca^{2+}]$ gradients in ventricular myocytes revealed by high speed digital imaging microscopy. *Proc. Natl. Acad. Sci. USA.* 93:5413–5418.

Kao, J.P., J. Alderton, R.Y. Tsien, and R.A. Steinhardt. 1990. Active involvement of Ca^{2+} in mitotic progression of Swiss 3T3 fibroblasts. *J. Cell Biol.* 111:183–196.

Lee, K.W., S.E. Webb, and A.L. Miller. 2003. Ca^{2+} released via $InsP_3$ receptors is required for furrow deepening during cytokinesis in zebrafish embryos. *Int. J. Dev. Biol.* 47:411–421.

Leung, C.F., S.E. Webb, and A.L. Miller. 1998. Calcium transients accompany ooplasmic segregation in zebrafish embryos. *Dev. Growth Differ.* 40:313–326.

Lu, K.P., and A.R. Means. 1993. Regulation of the cell cycle by calcium and calmodulin. *Endocr. Rev.* 14:40–48.

MacDonald, J.R. 1998. Nuclear calcium: transfer to and from the cytosol. *Biol. Signals Recept.* 7:137–147.

Mikoshiba, K. 1997. The InsP3 receptor and intracellular Ca^{2+} signaling. *Curr. Opin. Neurobiol.* 7:339–345.

Miller, A.L., R.A. Fluck, J.A. McLaughin, and L.F. Jaffe. 1993. Calcium buffer injections inhibit cytokinesis in *Xenopus* eggs. *J. Cell Sci.* 106:523–534.

Muto, A., and K. Mikoshiba. 1998. Activation of inositol 1,4,5-trisphosphate receptors induces transient changes in cell shape of fertilized *Xenopus* eggs. *Cell Motil. Cytoskeleton.* 39:201–208.

Muto, A., S. Kume, T. Inoue, H. Okano, and K. Mikoshiba. 1996. Calcium waves along the cleavage furrows in cleavage-stage *Xenopus* embryos and its inhibition by heparin. *J. Cell Biol.* 135:181–190.

Nixon, V.L., M. Levasseur, A. McDougall, and K.T. Jones. 2002. Ca^{2+} oscillations promote APC/C-dependent cyclin B1 degradation during metaphase arrest and completion of meiosis in fertilizing mouse eggs. *Curr. Biol.* 12:746–750.

Paddy, M.R., H. Saumweber, D.A. Agard, and J.W. Sedat. 1996. Time-resolved, in vivo studies of mitotic spindle formation and nuclear lamina breakdown in *Drosophila* early embryos. *J. Cell Sci.* 109:591–607.

Patel, R., M. Holt, R. Philipova, S. Moss, H. Schulman, H. Hidaka, and M. Whitaker. 1999. Calcium/calmodulin-dependent phosphorylation and activation of human Cdc25-C at the G2/M phase transition in HeLa cells. *J. Biol. Chem.* 274:7958–7968.

Poenie, M., J. Alderton, R.Y. Tsien, and R.A. Steinhardt. 1985. Changes of free calcium levels with stages of the cell division cycle. *Nature.* 315:147–149.

Riggs, B., W. Rothwell, S. Mische, G.R.X. Hickson, J. Matheson, T.S. Hays, G.W. Gould, and W. Sullivan. 2003. Actin cytoskeleton remodelling during early *Drosophila* furrow formation requires recycling endosomal components Nuclear-fallout and Rab11. *J. Cell Biol.* 163:143–154.

Rizzuto, R., and T. Pozzan. 2003. When calcium goes wrong: genetic alterations of a ubiquitous signaling route. *Nat. Genet.* 34:135–141.

Roegiers, F., A. McDougall, and C. Sardet. 1995. The sperm entry point defines the orientation of the calcium-induced contraction wave that directs the first phase of cytoplasmic reorganization in the ascidian egg. *Development.* 121:3457–3466.

Ross, C.A., J. Meldolesi, T.A. Milner, T. Satoh, S. Supattapone, and S.H. Snyder. 1989. Inositol 1,4,5-trisphosphate receptor localized to endoplasmic reticulum in cerebellar Purkinje neurons. *Nature.* 339:468–470.

Shuster, C.B., and D.R. Burgess. 2002. Targeted new membrane addition in the cleavage furrow is a late, separate event in cytokinesis. *Proc. Natl. Acad. Sci. USA.* 99:3633–3638.

Silver, R.B., R.D. Cole, and W.Z. Cande. 1980. Isolation of mitotic apparatus containing vesicles with calcium sequestration activity. *Cell.* 19:505–516.

Snow, P., and R. Nuccitelli. 1993. Calcium buffer injections delay cleavage in *Xenopus laevis* blastomeres by dissipating Ca^{2+} gradients. *J. Cell Biol.* 122:387–394.

Steinhardt, R.A., and J. Alderton. 1988. Intracellular free calcium rise triggers nuclear envelope breakdown in the sea urchin embryo. *Nature.* 332:364–366.

Steinhardt, R.A., D. Epel, E.J. Carroll, and R. Yanagimachi. 1974. Is calcium ionophore a universal activator for unfertilised eggs? *Nature.* 252:41–43.

Sullivan, W., and W. Theurkauf. 1995. The cytoskeleton and morphogenesis of the early *Drosophila* embryo. *Curr. Opin. Cell Biol.* 7:18–22.

Sunkel, C.E., and D.M. Glover. 1988. Polo, a mitotic mutant of *Drosophila* displaying abnormal spindle poles. *J. Cell Sci.* 89:25–38.

Takeuchi, H., M. Oike, H.F. Paterson, V. Allen, T. Kanematsu, Y. Ito, C. Erneux, M. Katan, and M. Hirata. 2000. Inhibition of Ca^{2+} signalling by p130, a phospholipase-C-related catalytically inactive protein: critical role of the p130 pleckstrin homology domain. *Biochem. J.* 349:357–368.

Takuwa, N., W. Zhou, and Y. Takuwa. 1995. Calcium, calmodulin and cell cycle progression. *Cell. Signal.* 7:93–104.

Terasaki, M., and L.A. Jaffe. 1991. Organization of the sea urchin egg endoplasmic reticulum and its reorganization at fertilization. *J. Cell Biol.* 114:929–940.

Tombes, R.M., and G.G. Borisy. 1989. Intracellular free calcium and mitosis in mammalian cells: anaphase onset is calcium modulated, but is not triggered by a brief transient. *J. Cell Biol.* 109:627–636.

Tombes, R.M., C. Simerly, G.G. Borisy, and G. Schatten. 1992. Meiosis, egg activation and nuclear envelope breakdown are differentially reliant on Ca^{2+}, whereas germinal vesicle breakdown is Ca^{2+} independent in the mouse oocyte. *J. Cell Biol.* 117:799–811.

Török, K., M. Wilding, L. Groigno, R. Patel, and M. Whitaker. 1998. Imaging the spatial dynamics of calmodulin activation during mitosis. *Curr. Biol.* 8:692–699.

Twigg, J., R. Patel, and M. Whitaker. 1988a. Translational control of $InsP_3$-induced chromatin condensation during the early cell cycles of sea urchin embryos. *Nature.* 332:366–369.

Twigg, J., R. Patel, and M. Whitaker. 1988b. Translational control of $InsP_3$-induced chromatin condensation during the early cell cycles of sea urchin embryos. *Nature.* 332:366–369.

Uchiyama, T., F. Yoshikawa, A. Hishida, T. Furuichi, and K. Mikoshiba. 2002. A novel recombinant hyperaffinity inositol 1,4,5-trisphosphate (IP(3))

absorbent traps IP(3), resulting in specific inhibition of IP(3)-mediated calcium signaling. *J. Biol. Chem.* 277:8106–8113.

Van der Meer, J.M., and L.F. Jaffe. 1983. Elemental composition of the perivitelline fluid in early *Drosophila* embryos. *Dev. Biol.* 95:249–252.

Walker, D.S., N.J.D. Gower, S. Ly, G.L. Bradley, and H.A. Baylis. 2002. Regulated disruption of inositol 1,4,5-trisphosphate signalling in *Caenorhabditis elegans* reveals new functions in feeding and embryogenesis. *Mol. Biol. Cell.* 13:1329–1337.

Webb, D.J., and R. Nuccitelli. 1985. Fertilization potential and electrical properties of the *Xenopus laevis* egg. *Dev. Biol.* 107:395–406.

Webb, S.E., and A.L. Miller. 2003. Calcium signalling during embryonic development. *Nat. Rev. Mol. Cell Biol.* 4:539–551.

Webb, S.E., K.W. Lee, E. Karplus, and A.L. Miller. 1997. Localized calcium transients accompany furrow positioning, propagation, and deepening during the early cleavage period of zebrafish embryos. *Dev. Biol.* 192:78–92.

Whitaker, M., and M.G. Larman. 2001. Calcium and mitosis. *Semin. Cell Dev. Biol.* 12:53–58.

Wilding, M., E.M. Wright, R. Patel, G. Ellis-Davies, and M. Whitaker. 1996. Local perinuclear signals associated with mitosis-entry in early sea urchin embryos. *J. Cell Biol.* 135:191–199.

Yoshikawa, S., T. Tanimura, A. Miyawaki, M. Nakamura, M. Yuzaki, T. Furuichi, and K. Mikoshiba. 1992. Molecular cloning and characterization of the inositol 1,4,5-trisphosphate receptor in *Drosophila melanogaster*. *J. Biol. Chem.* 267:16613–16619.

Zalokar, M., and I. Erk. 1976. Division and migration of nuclei during early embryogenesis of *Drosophila melanogaster*. *J. Microsc. Biol. Cell.* 25:97–106.